Supporting Information

Grain Boundaries and Their Impact on Li Kinetics in Layered-Oxide Cathodes for Li-Ion Batteries

Xiaomei He,[†,‡] Hong Sun, [‡] Xiangdong Ding,*,[†] and Kejie Zhao*,[‡]

[†]State Key Laboratory for Mechanical Behavior of Materials, Xi'an Jiaotong University, Xi'an, 710049, China

[‡]School of Mechanical Engineering, Purdue University, West Lafayette, IN 47907, USA

*Corresponding author. E-mails: dingxd@mail.xjtu.edu.cn (X. D.) and kjzhao@purdue.edu (K. Z.)

Computational Methods

Supercell model: The NMC supercells of various GB structures are constructed using the coincidence site lattice (CSL) theory.[1] Four symmetric tilt GB models are built, namely, $\Sigma 2(1\bar{1}0\bar{4})[\bar{1}\bar{1}20]$, $\Sigma 3(\bar{1}10\bar{2})[\bar{1}\bar{1}20]$, $\Sigma 5(1\bar{1}0\bar{1})[\bar{1}\bar{1}20]$, and $\Sigma 9(\bar{1}10\bar{4})[\bar{1}\bar{1}20]$, as shown in Figure S1 a-d. All the atomic structures are periodic in all the directions and contain 240 atoms. The notation Σ is defined as the ratio of the coincidence unit cell volume to the primitive unit cell volume.[1] Note that layered-oxide NMC has a hexagonal (space group $R\bar{3}m$) structure. Except for the rotations about [0001], the exact CSL boundaries are obtained only when $(c/a)^2$ is a rational number.[2] In this study, Σ values are approximated near-CSL boundaries.

GB energy calculation: After structural optimization, the atomic structures are shown in Figure S1 a1-d1. The GB energy, γ_{GB}, is determined by

$$\gamma_{GB} = \frac{E_{GB} - E_{bulk}}{2A},\qquad(1)$$

where E_{GB} is the energy of the supercell containing GB, E_{bulk} the energy of the bulk supercell with an equal number of atoms, and A the area of the interface between the bi-crystal grains.

Structural optimization: To obtain an optimized and stable GB structure. AIMD annealing and energy relaxation are carried out. DFT + U is adopted to correct the Coulombic repulsion of the transition-metal elements. The Hubbard U values for Ni, Mn, and Co are taken from previous studies,[3,4] with U - J being 6.70 eV, 4.20 eV, and 4.91 eV, respectively. To incorporate the effect of the van der Waals (vdW)

interactions between layers, the DFT+D3 method with Becke-Jonson damping is employed.[5,6] In AIMD modeling, the NVT ensemble with a Nose-Hoover thermostat is used to regulate the temperature. The time-step Δt = 2 fs and single Γ point Brillouin zone sampling are used. AIMD is conducted in the two main processes for each GB structure. First, annealing is performed at T = 800 K for 4 ps to facilitate the local rearrangement of atoms. After annealing, the systems are quenched sequentially from 800 K to 0 K with a cooling rate of 8×10^{14} K s^{-1}, and followed by 1 ps of NVT simulation at T = 0 K to equilibrate the system. The final structural relaxation at T = 0 K is performed with DFT calculations. The lattice parameters determined under DFT+U+D3 are in excellent agreement with the experimental results as elaborated in the previous studies.[7,8]

Calculation of Li-ion migration energy barrier: Li diffusion and the corresponding energy barriers are calculated using the climbing image nudged elastic band (CI-NEB) method, a complementary to the NEB method.[9,10] The CI-NEB path requires the initial and final states of diffusion as input and generates the intermediate states by a linear interpolation of the atomic coordinates. In our calibration study, we find that pure PBE functional performs better compared to the +U method which causes over-localization of the electron density at the nuclei along the diffusion pathway. This finding is consistent with the previous reports.[8,11–13] In the CI-NEB calculations, only the atomic positions in the supercell are allowed to relax while the overall lattice parameters are fixed. It is worth noting that the vdW interactions between NMC layers might become important at low Li concentrations; nevertheless, the current study of Li diffusion is performed at the fully lithiated state. In addition, the lattice parameters are fixed during structural optimization with the DFT+U+D3 method. Our results show that the dispersion corrections play a negligible effect, and hence they are not included in the CI-NEB calculations.
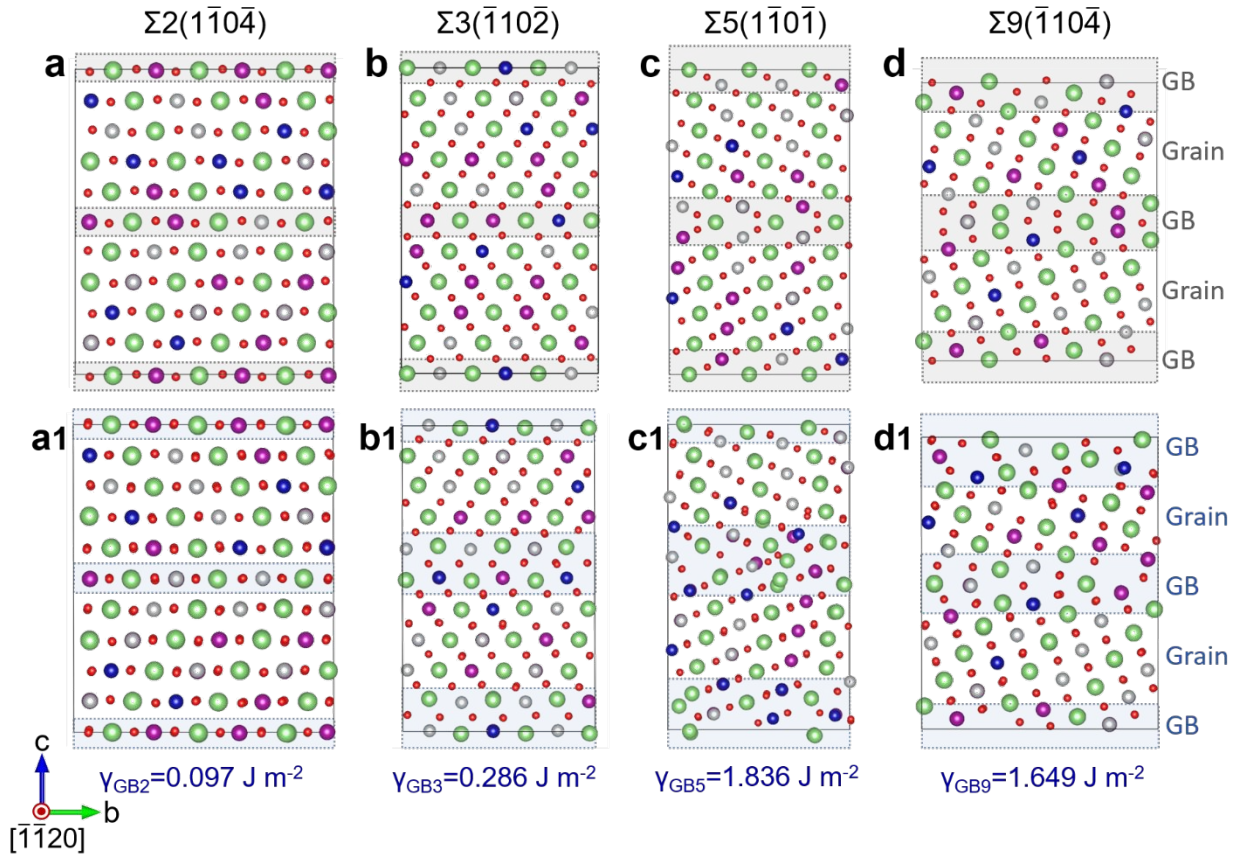
Figure S1. NMC supercells of symmetric tilt GBs and the atomic structures after energy minimization. Panels (a)-(d) show the coincident site lattices of $\Sigma 2(1\bar{1}0\bar{4})$, $\Sigma 3(\bar{1}10\bar{2})$, $\Sigma 5(1\bar{1}0\bar{1})$, and $\Sigma 9(\bar{1}10\bar{4})$ GBs, respectively. Panels (a1)-(d1) are the optimized structures with the calculated GB energies.

Table S1 Structural parameters of the initial CSL GB models

| GB	$\Sigma 2(1\bar{1}0\bar{4})$	$\Sigma 3(\bar{1}10\bar{2})$	$\Sigma 5(1\bar{1}0\bar{1})$	$\Sigma 9(\bar{1}10\bar{4})$
GB plane	$(1\bar{1}0\bar{4})$	$(\bar{1}10\bar{2})$	$(1\bar{1}0\bar{1})$	$(\bar{1}10\bar{4})$
Rotation axis	$[\bar{1}\bar{1}20]$	$[\bar{1}\bar{1}20]$	$[\bar{1}\bar{1}20]$	$[\bar{1}\bar{1}20]$
Rotation angle	69.6°	38.4°	19.9°	69.6°
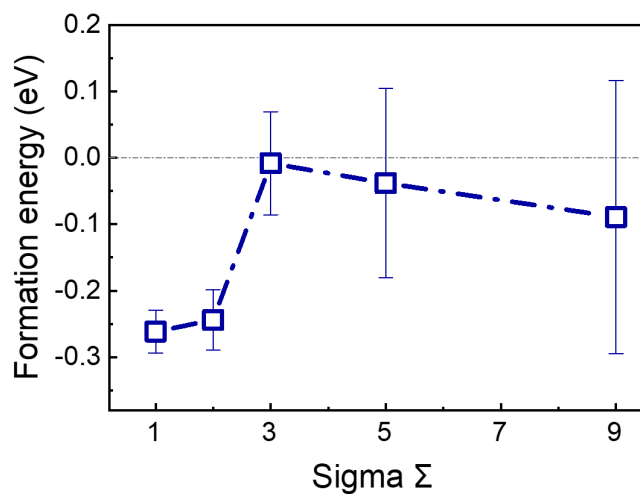
Figure S2. Li-vacancy formation energy as a function of the Σ values in NMC lattice. The error bars represent the standard deviation.
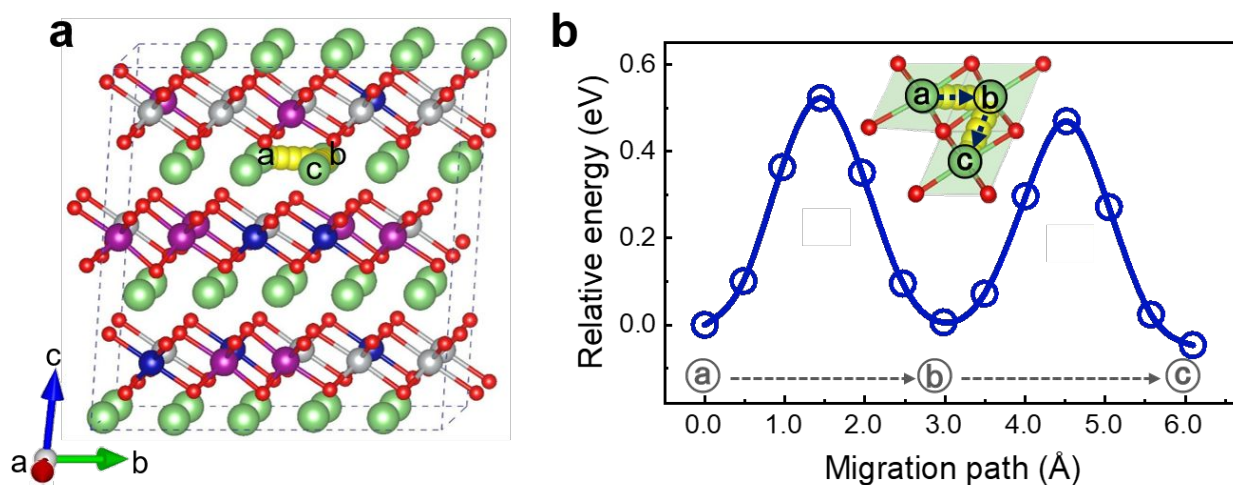

Figure S3. Li diffusion pathway in the bulk NMC. (a) The atomic structure and the trajectory of Li hopping between two adjacent Li sites. (b) The energy barrier calculated by the CI-NEB method. The average energy barrier is $E_{ave} = 0.505$ eV. Inset shows the diffusion trajectory from the sites a to c in the energy profile.
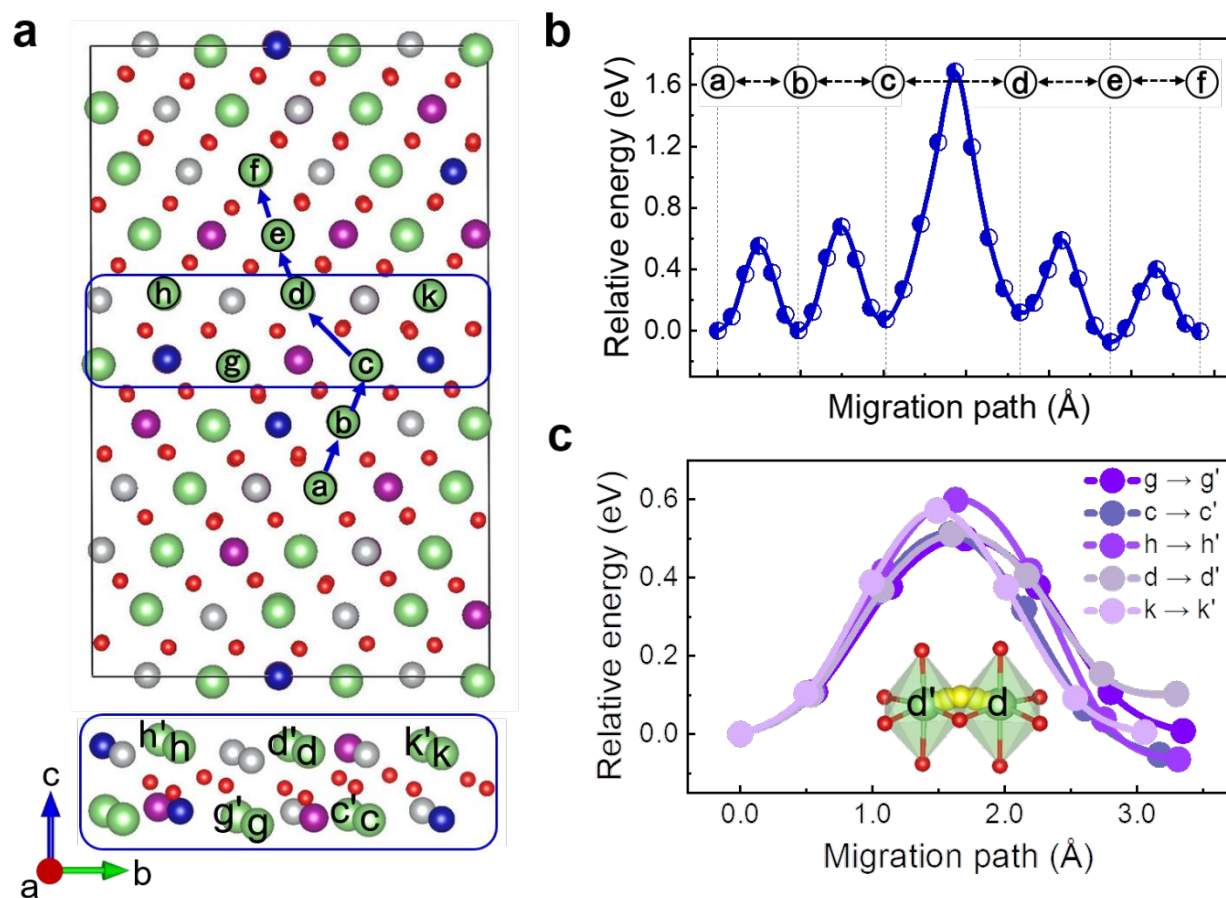
Figure S4. Li diffusion pathways and the associated energy profiles in the vicinity of the Σ3 GB. (a) Li sites involved in each sub-step across (upper panel) and within (lower panel) the GB plane. (b) The energy landscape for Li transport across the GB. (c) The relatively uniform energy barriers for Li diffusion within the GB plane. Inset shows an example migration path.
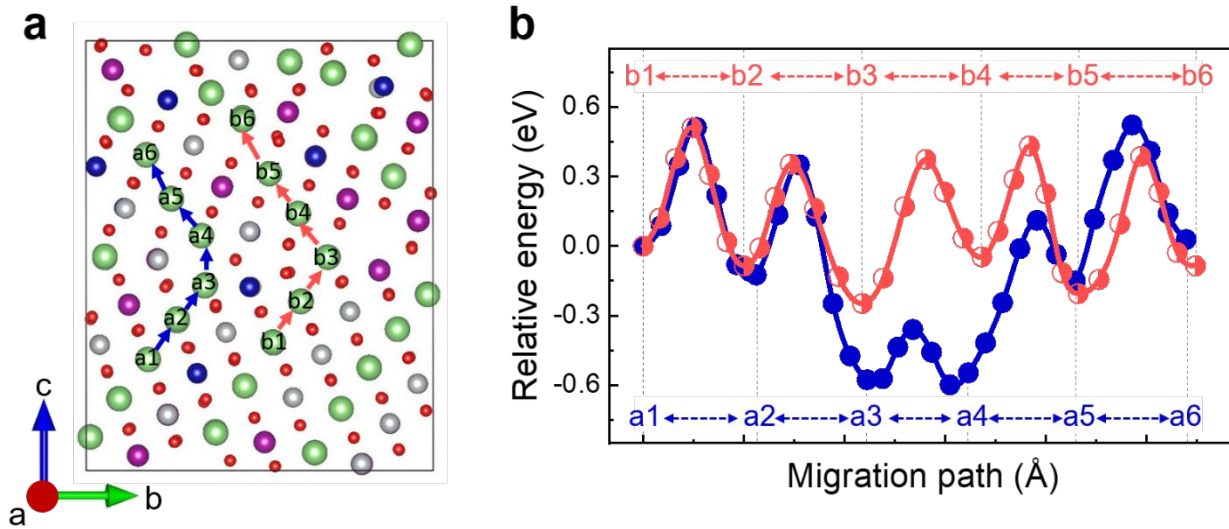
Figure S5. Li migration near the Σ9 GB. (a) Two possible Li diffusion pathways (a1-a6 and b1-b6) perpendicular to the GB plane. (b) Energy profiles for Li hopping along the pathyways outlined in (a).
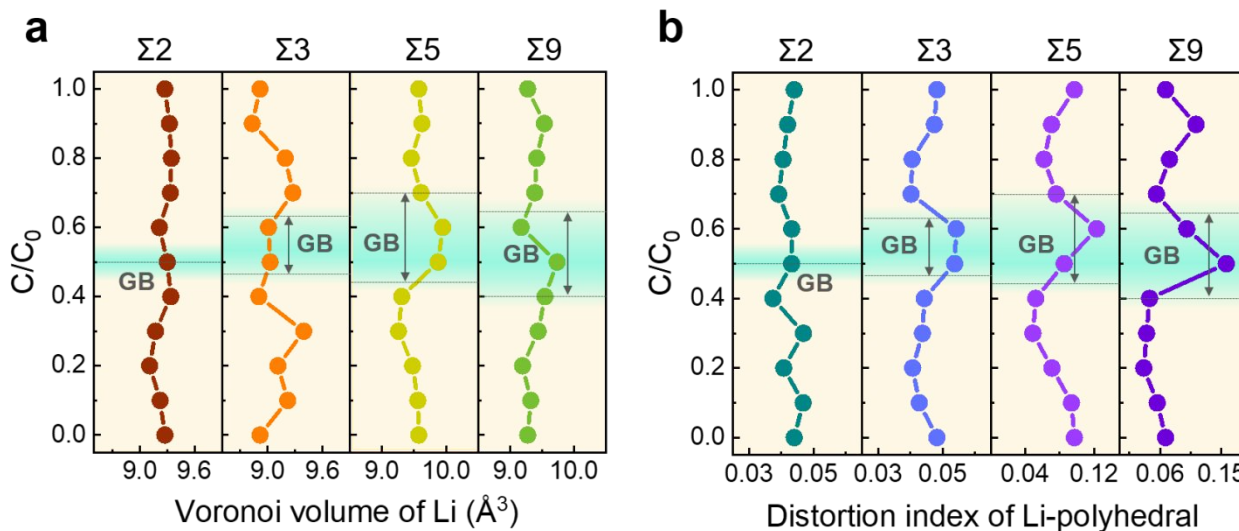
Figure S6. Local Voronoi volume of Li (V_{Li}) and the distortion index of Li-polyhedral (d_{Li}) in different GB configurations. The vertical axis represents the distance along the *c*-axis of the GB structures as shown in Figure S1. (a) and (b) show V_{Li} and d_{Li} determined by averaging the values of each Li-polyhedral layer along the *b*-axis, respectively. The GB locations are marked by the green shaded color.
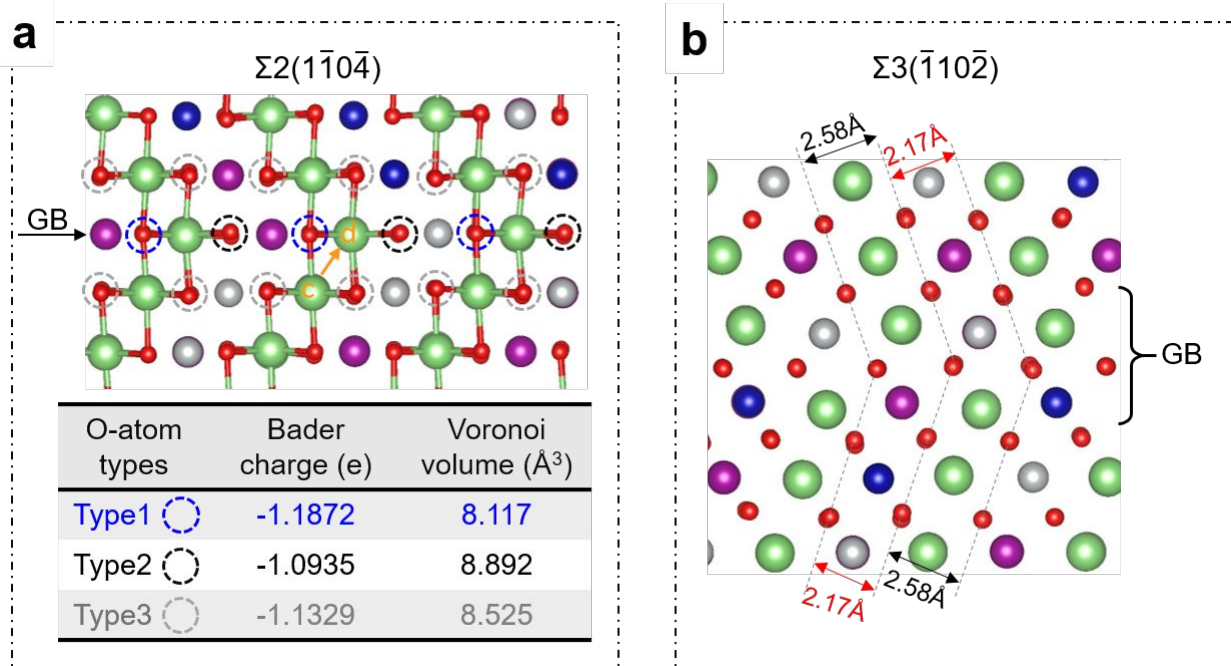
Figure S7 Configurational features of the Σ2 and Σ3 GBs. (a) Bader charge and Voronoi volume analysis of O atoms in the Σ2 GB structure. O atoms can be divided into three types. Specifically, Type1 (blue circles at GB) is surrounded by 4 Li atoms and 2 TM atoms (4Li+2TM), Type2 (black circles at GB) by 2Li+4TM, and Type3 (grey circles in the bulk) by 3Li+3TM. The Type1 O atoms have the most negative Bader charge and the smallest Voronoi volume, Type2 O exhibit the least negative Bader charge and the largest Voronoi volume, and Type3 in between. Li diffusion from the sites c to d across the GB is marked in (a), where the Type1 O atom near the transition state decreases the energy barrier due to the more negative Bader charge which attracts Li and the smaller Voronoi volume which provides a larger space for Li migration. (b) Li slab and TM slab are adjoined at the GB which induces lattice mismatch for the Σ3 GB. The decreased TM slab space reduces the Li slab space, resulting in the smaller Li Voronoi volume near the GB and a higher Li migration barrier.

Reference

(1)   Grain Boundaries: *From Theory to Engineering*; Priester, L.; Springer: New York, 2012.

(2)   Bruggeman, G. A., Bishop, G. H., Hartt, W. H. In *The nature and behavior of grain boundaries*; Hu, H., Eds.; Springer: New York, **1972**; pp 83–122.

(3)   Zhou, F.; Cococcioni, M.; Marianetti, C. A.; Morgan, D.; Ceder, G. First-Principles Prediction of Redox Potentials in Transition-Metal Compounds with LDA+ U. *Phys. Rev. B* **2004**, *70*, 235121.

(4)   Sun, H.; Zhao, K. Electronic Structure and Comparative Properties of $LiNi_xMn_yCo_zO_2$ Cathode Materials. *J. Phys. Chem. C* **2017**, *121*, 6002–6010.

(5)   Grimme, S.; Antony, J.; Ehrlich, S.; Krieg, H. A Consistent and Accurate Ab Initio Parametrization of Density Functional Dispersion Correction (DFT-D) for the 94 Elements H-Pu. *J. Chem. Phys.* **2010**, *132*, 154104.

(6)   Grimme, S.; Ehrlich, S.; Goerigk, L. Effect of the Damping Function in Dispersion Corrected Density Functional Theory. *J. Comput. Chem.* **2011**, *32*, 1456–1465.

(7)   Aykol, M.; Kim, S.; Wolverton, C. Van Der Waals Interactions in Layered Lithium Cobalt Oxides. *J. Phys. Chem. C* **2015**, *119*, 19053–19058.

(8)   Dixit, M.; Kosa, M.; Lavi, O. S.; Markovsky, B.; Aurbach, D.; Major, D. T. Thermodynamic and Kinetic Studies of $LiNi_{0.5}Co_{0.2}Mn_{0.3}O_2$ as a Positive Electrode Material for Li-Ion Batteries Using First Principles. *Phys. Chem. Chem. Phys.* **2016**, *18*, 6799–6812.

(9)   Henkelman, G.; Jónsson, H. Improved Tangent Estimate in the Nudged Elastic Band Method for Finding Minimum Energy Paths and Saddle Points. *J. Chem. Phys.* **2000**, *113*, 9978–9985.

(10) Henkelman, G., Jóhannesson, G., Jónsson, H. In *Theoretical Methods in Condensed Phase Chemistry*; Schwartz, S. D., Eds.; Springer: Dordrecht, 2002; Vol. 5, pp 269–302.

(11) Urban, A.; Seo, D.-H.; Ceder, G. Computational Understanding of Li-Ion Batteries. *npj Comput.Mater.* **2016**, *2*, 16002.

(12) Chakraborty, A.; Kunnikuruvan, S.; Kumar, S.; Markovsky, B.; Aurbach, D.; Dixit, M.; Major, D. T. Layered Cathode Materials for Lithium-Ion Batteries: Review of Computational Studies on $LiNi_{1-x-y}Co_xMn_yO_2$ and $LiNi_{1-x-y}Co_xAl_yO_2$. *Chem. Mater.* **2020**, *32*, 915–952.

(13) Mueller, T.; Hautier, G.; Jain, A.; Ceder, G. Evaluation of Tavorite-Structured Cathode Materials for Lithium-Ion Batteries Using High-Throughput Computing. *Chem. Mater.* **2011**, *23*, 3854–3862.